FINAL REPORT

DEVELOPMENT OF GALLIUM ARSENIDE
SOLAR CELLS

Contract No. 953270

Submitted to:

Jet Propulsion Laboratory
California Institute of Technology
Pasadena, California

February 1973

ION/PHYSICS CORPORATION IPC

TABLE OF CONTENTS

ii

LIST OF ILLUSTRATIONS

SECTION 1
SUMMARY

This is the final report on a research and development program which had the objective of exploring the potential of ion implantation as a means to the development of high efficiency gallium arsenide solar cells.

Section 2 of this report summarizes the results of computer calculations of GaAs cell characteristics, based on a model which includes the effects of surface recombination, junction space-charge region recombination, and built-in fields produced by non-uniform doping in the surface region. P/N cells were found to be superior to N/P cells, and an optimized structure was found for which the AMO efficiency (before surface reflectivity corrections) was calculated to be 23%.

Section 3 summarizes the fabrication technology developed under this program. In addition to techniques for the implantation of zinc and beryllium and the annealing of the implanted layers, improved techniques for surface preparation, contacting, and etching were developed. These techniques were adequate for the fabrication of the structure which was calculated to be optimum.

Section 4 summarizes the results of electrical and optical measurements on the samples produced during this program. Measured AMO efficiencies on the best samples were more than a factor of two lower than the calculated values. The measurements were analyzed to determine the cause of this discrepancy; we found that the cause was extremely low minority carrier lifetime in the surface region, approximately two orders of magnitude lower than the values assumed in the calculation, which were based on measurements on boat-grown samples. The low lifetime was tentatively ascribed to the presence of a high concentration of electrically active oxygen in the surface region. The source of the oxygen contamination was not found, but a method of gettering oxygen from implanted samples is proposed. Time did not permit experimental work on oxygen gettering.

SECTION 2
CALCULATIONS OF GaAs CELL CHARACTERISTICS

The first step in the program was the development of a means for calculation of the characteristics of GaAs cells, in order to determine the optimum cell structure. A computer program was written to solve the equations derived by Ellis and Moss,[1] and the recent literature on GaAs was searched to determine the best available values for the required physical parameters.

The properties of GaAs differ considerably from those of Si, with the result that the optimum structure for a GaAs solar cell is significantly different than for a Si solar cell. The first important difference is in the spectral absorption coefficient $\propto$. Silicon is an indirect band-gap material; the absorption coefficient exhibits two absorption edges at 1.1 eV (indirect transitions) and about 3 eV (direct transitions). For photon energies between these values, which account for almost all of the photo-generated current in a Si solar cell, the absorption coefficient is of the order of 10^3 cm^{-1}. Gallium arsenide is a direct band-gap material; the absorption coefficient[2] is about 10^4 cm^{-1} at a photon energy corresponding to the band-gap (1.43 eV at 300 °K, corresponding to a wavelength of 0.867 micrometers), and increases smoothly to about 10^5 cm^{-1} at 4 eV (See Figure 1). Absorption of solar energy therefore occurs over distances of the order of 50 times smaller in GaAs than in Si. An important consequence is that, even for the shallowest practicable junctions, a major part of the photo-response is contributed by the surface layer. In the design of a GaAs cell, optimization of the surface layer characteristics (minority carrier lifetime, doping profile, and surface recombination velocity) is the major technical problem, while in Si base region characteristics are most important and surface effects can be minimized effectively by a shallow junction.

A second important difference is that the minority carrier lifetimes in commercially-available boat-grown GaAs crystals appear to be constant for doping concentrations up to the edge of degeneracy (Figures 2 and 3). Above acceptor concentrations of 10^{19} cm^{-3} in P-type material, or donor concentrations
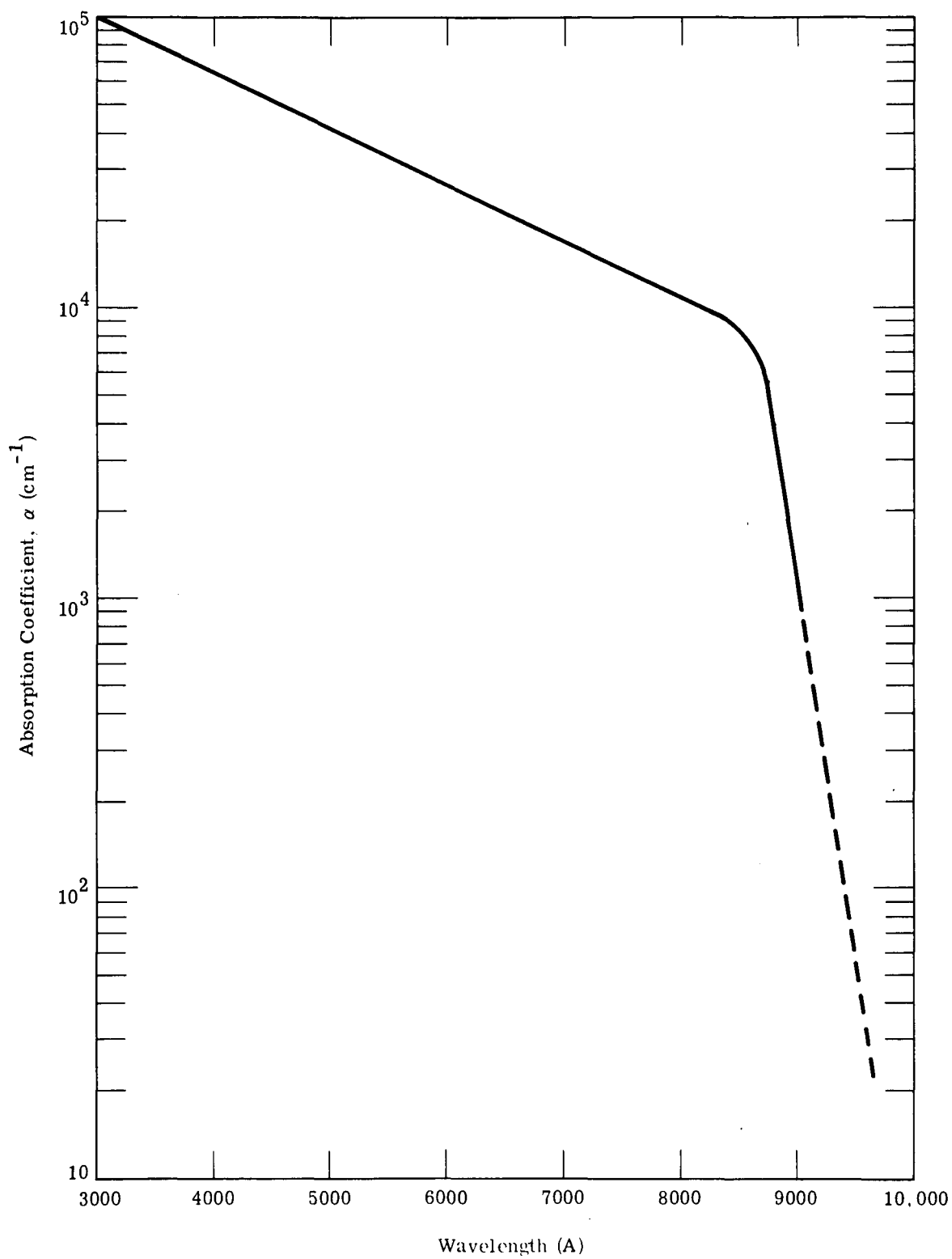
Figure 1.   Absorption Coefficient of GaAs as a Function
of Wavelength.

1-6334
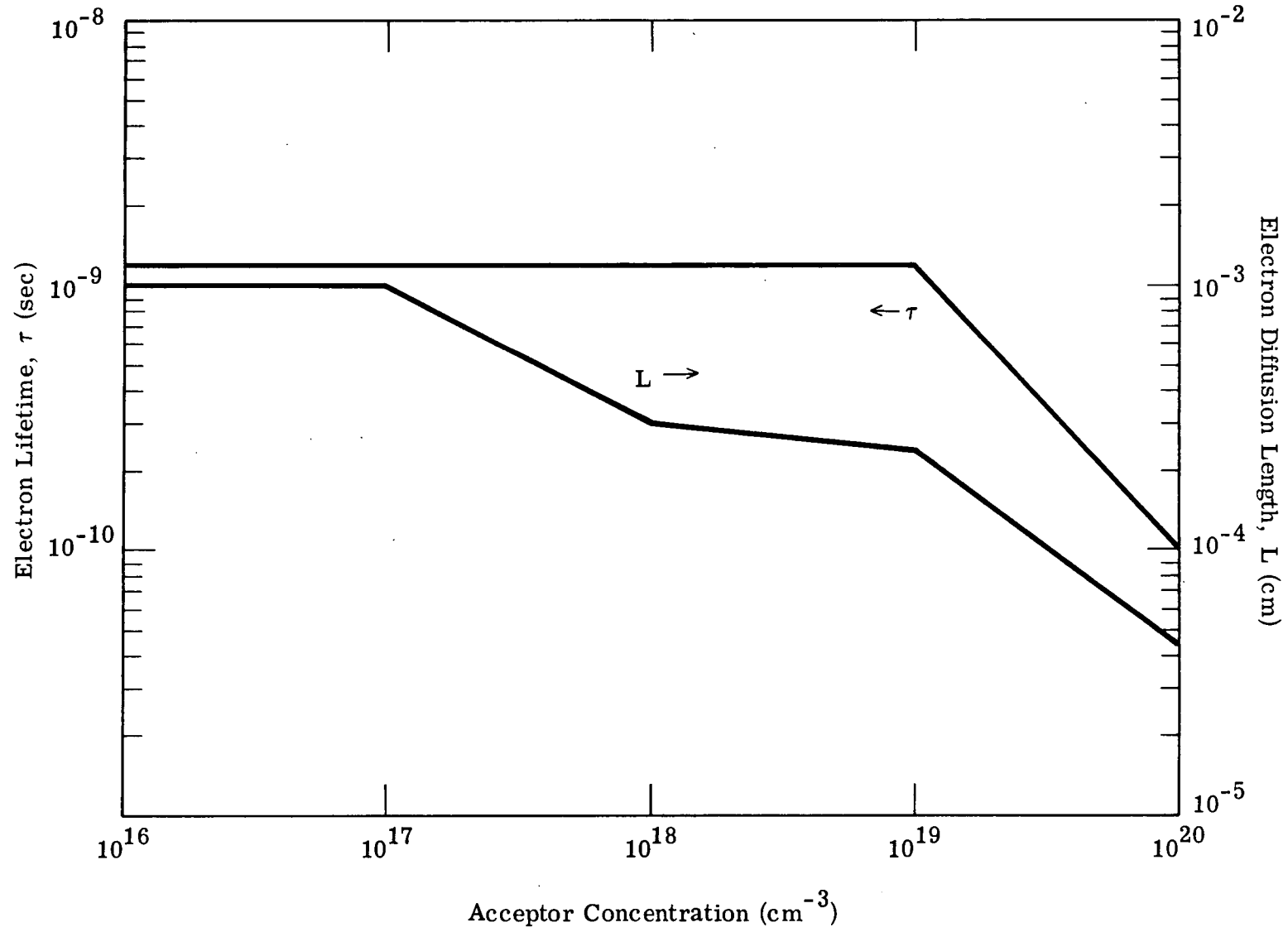
Figure 2.   Doping Dependence of Electron Diffusion Length and Lifetime in p-type GaAs.
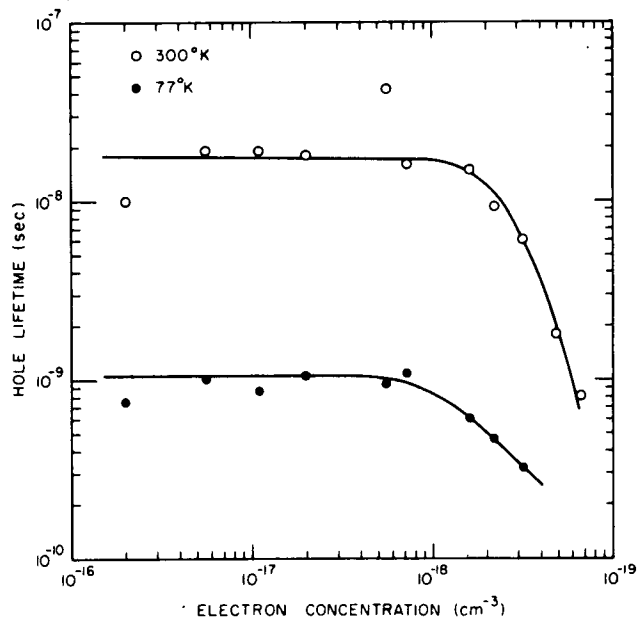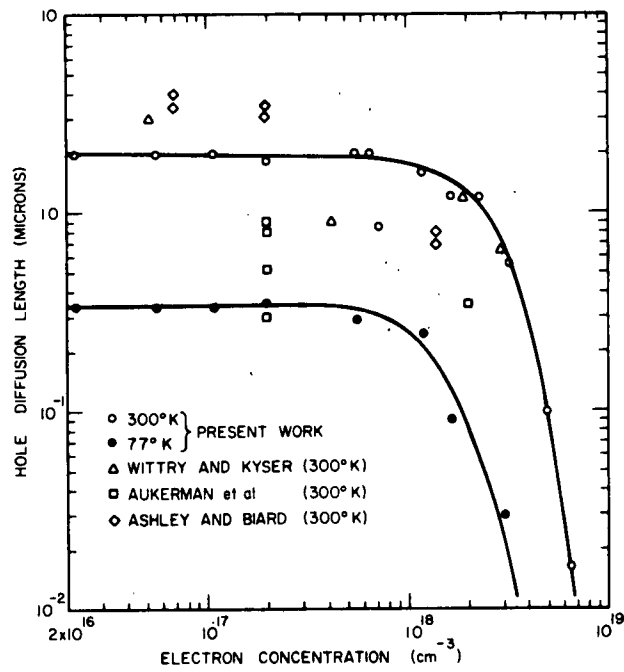
Figure 3. Doping Dependence of Hole Diffusion Length and Lifetime in n-type GaAs. (After Hwang, J. Appl. Phys. 42, 4408; 1971).

5

of 10^{18} cm^{-3} in N-type material, the minority carrier lifetime drops rapidly due to the fact that recombination is increased by band-tailing effects. These concentrations therefore represent the maximum doping concentrations which should be used in a GaAs solar cell. At these concentrations, both the hole and electron minority carrier diffusion lengths are approximately 2 micrometers. Although this value is lower than the values observed in silicon, the collection efficiency of a solar cell depends on the $\propto$L product; because of the high value of $\propto$ in GaAs, the collection efficiency in a heavily doped GaAs cell should equal or exceed the values observed in 10 ohm-cm Si cells.

A third important difference between GaAs and Si is the high electron mobility and high mobility ratio μ_n/μ_p in heavily-doped GaAs.[3] At an impurity concentration of 10^{19} cm^{-3}, μ_n is 1600 cm^2/v-sec and μ_n/μ_p is 20. This leads to important differences between P/N and N/P GaAs cells. The built-in field resulting from the doping gradient in the surface region has far more effect on the electrons in a P/N cell than on the holes in an N/P cell; in fact, for junction depths less than about 0.25 micrometers, the electrons in the surface region of a P/N cell experience a built-in field sufficiently great to cause them to drift at their limiting velocity of about 10^7 cm/sec. Therefore bulk recombination in the surface region of a P/N cell, for junction depths up to 1 micrometer, is negligible provided that the electron lifetime exceeds 10^{-10} seconds. The built-in field also reduces the effect of high surface recombination velocity; for values of S of 10^5 cm/sec or less, surface recombination has a negligible effect on the characteristics of a P/N cell. The maximum physically possible value for S is 10^7 cm/sec;[4] even this value of S leads to a reduction of short-circuit current of only about 10% for a junction depth of 0.25 micrometers or less. On the other hand, for N/P cells the limiting velocity for holes is reached at much higher fields, which cannot be achieved in a practical structure. Therefore, surface region bulk lifetime must be about an order of magnitude greater, and surface recombination velocity about two orders of magnitude lower, in an N/P cell to achieve the same high value of surface region collection efficiency calculated for an optimum P/N cell.

The results of our computer calculations illustrate the above conclusions. Figures 4 and 5 summarize results for P/N and N/P cells respectively. The surface doping concentration was taken as the optimum value (N_A = 10^{19} cm^{-3} for P/N cells, N_D = 10^{18} cm^{-3} for N/P cells). An exponential grading in the surface region was assumed; the difference between this profile and the actual (Gaussian) profile of an implanted layer is negligible at the lower values of junction depth and just noticeable at 1.0 micrometer. The surface recombination velocity was taken as 10^5 cm/sec; higher values (up to the maximum value of 10^7 cm/sec) will have little effect on the P/N cell results but will substantially lower the N/P values.

It can be seen that the computed values of open-circuit voltage are substantially lower for N/P cells, as compared to P/N cells of the same base doping. In these calculations, cell open-circuit voltage was calculated by computing the cell voltage at which the total recombination current equaled the photo-generated current. The total recombination current includes four components:

(1)   surface recombination

(2)   surface region bulk recombination (as modified by the built-in field)

(3)   base region bulk recombination

(4)   junction space-charge region recombination

In P/N cells, the first and second of these components are negligible and the third and fourth are of the same order of magnitude. In N/P cells, all components are larger than in an equivalently doped P/N cell: the first and second because of the reduced effect of the built-in field, as mentioned above; the third because of the higher diffusion coefficient of electrons; and the fourth because of the lower built-in voltage of N/P junctions compared to equivalently doped P/N junctions,[5] which is also a consequence of the high electron mobility in GaAs. The open-circuit voltage is therefore computed to be lower.

It also is clear that the efficiency of an N/P cell drops off rapidly with increasing junction depth, while the P/N cell results show a broad maximum
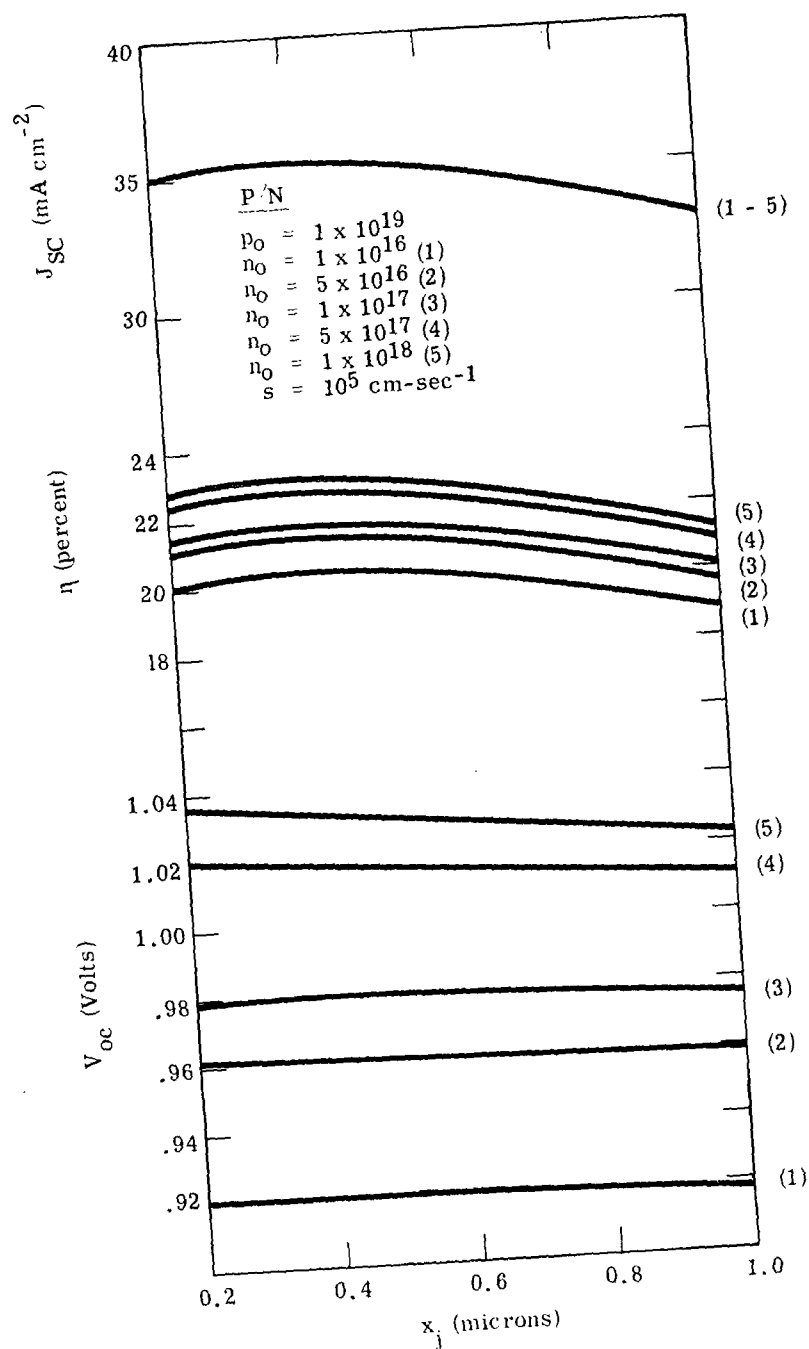
Figure 4. Variation of Calculated Efficiency, Short-Circuit Current and Open-Circuit Voltage with Junction Depth for a Range of Base Region Concentrations.

1-6343

8
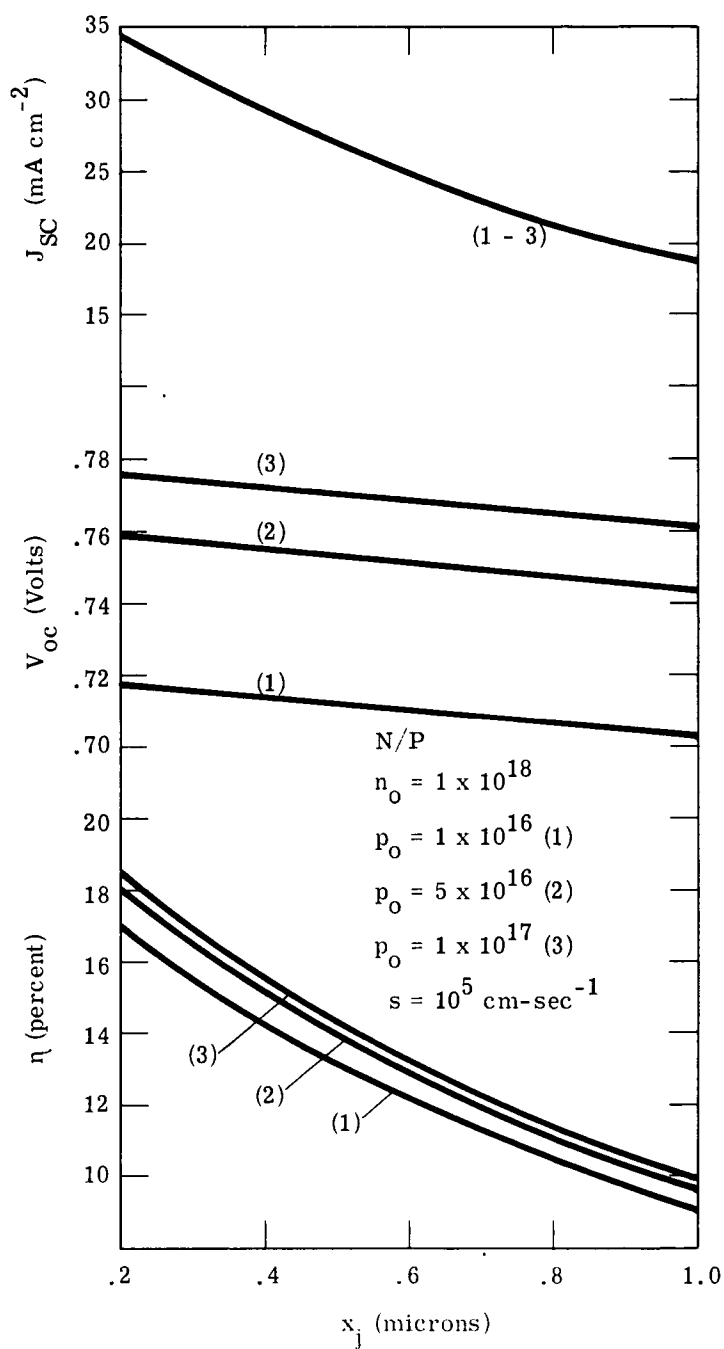
Figure 5. Calculated Values of Efficiency, Short-Circuit Current and Open-Circuit Voltage versus Junction Depth for Several Values of Base Doping.

1-6346

9

in efficiency at about 0.4 micrometers. The N/P cell is therefore much more difficult to fabricate. Although the surface layer sheet resistance of the N/P cell is one-half that of the P/N cell for the same junction depth, the sheet resistance of the P/N cell is sufficiently low so that negligible degradation of curve factor would result if a 14-finger contact was used, even for a junction depth of 0.2 micrometers.

The efficiency values given in Figures 4 and 5 are not corrected for surface reflection losses, or for the area covered by the front contact. According to Siebert,[6] the integrated reflectivity of an optimized single-layer anti-reflective coating results in a loss of 6.8% of the theoretical short-circuit current. The area covered by the IPC 14-finger contact is 5% of the total cell area (4 cm^2). Applying these correction factors, an efficiency greater than 20% is still seen to be possible for an optimized GaAs solar cell.

In summary, the optimum GaAs solar cell design is calculated to be:

- P/N polarity
- base doping 10^{18} cm^{-3}
- graded surface region; surface acceptor concentration 10^{19} cm^{-3}
- junction depth 0.4 micrometers

SECTION 3
CELL FABRICATION TECHNIQUES

Ion implantation was chosen as the technique to be used to fabricate the optimized structure described above. Work done on zinc implants into GaAs, performed prior to this program, had shown that implanted layers with the required sheet resistance and junction depth could be easily and reproducibly fabricated in this way. Also, good diode I-V characteristics had been obtained.

In the course of this program, beryllium was found to be superior to zinc as an implanted acceptor, because the lower mass of the Be^+ ion permitted implantation at lower voltage, greatly reducing the amount of lattice damage produced by implantation. In addition to the fact that the use of Be^+ instead of Zn^+ brought the required implantation voltage down into the range of commercially available production ion implantation equipment, the Be-implanted layers were found to anneal at lower temperatures and gave lower sheet resistances for the same dose.

In addition, significant improvements were made during the program in the areas of materials preparation, contact formation, and post-contact surface treatment.

3.1 Materials and Surface Preparation

Although the optimum value of base doping for the P/N cell was calculated to be 10^{18} cm^{-3}, it is difficult to grow GaAs crystals of such high dopant concentration which exhibit low etch pit density and freedom from dopant segregation effects. After consultation with materials vendors, we decided to order our GaAs crystals doped with tellurium to 2×10^{17} cm^{-3}. This material had been found to be optimum for the fabrication of electroluminescent diodes. A few implants at the beginning of the program were done into material doped to 1×10^{16} cm^{-3}, which was on hand. All material was boat-grown, approximately $4 \times 2 \times .05$ cm in dimensions, with an etch pit density less than 1000 cm^{-2}.

Initially, the sliced wafers were prepared for implantation by chem-mechanical polishing on a Politex pad with 2% sodium hypochlorite solution, followed by a 1 minute etch in 5% bromine in methanol. In some cases several polishing/etching cycles were necessary to produce a mirror finish. After our initial results showed non-uniform junction characteristics, we reviewed this process and found that the polishing step in some instances created deep scratches not apparent to the naked eye. The etching step did not always bring out these scratches because the etching time was insufficient.

After further experimentation, a revised procedure was developed which consistently produced surfaces which appeared to be damage-free. This procedure is:

(1)   Etch A and B faces in a solution of 1% by volume of bromine in methanol for 1 minute.

(2)   Mount A face down on glass slide and lap B face to a uniform finish with 5 micron diamond grit.

(3)   Chem-mechanical polish B face on Pellon cloth by hand using 1% by volume bromine in methanol. Complete to high polish finish.

(4)   Etch in 1% by volume bromine in methanol for 1 minute and rinse thoroughly in methanol.

(5)   Etch in 1 H_2SO_4 : 1 H_2O_2 : 1 H_2O solution for 30 seconds and rinse thoroughly in deionized water.

(6)   Dismount slice. Clean and vapor degrease in trichloro-ethylene.

3.2   Zinc Implantation

Zinc ions were produced in an arc discharge source in the terminal of a 2 MeV Van de Graaff accelerator. The ion beam was magnetically analyzed and electrostatically scanned over a 5 x 5 cm area. Implantations were per-formed over the energy ranges 200 to 1400 keV and the dose range 5 x 10^{14} to

5×10^{15} ions/cm^2. Samples were maintained at room temperature during implantation.

Annealing was performed at temperatures between 400 °C and 800 °C. Samples annealed at 600 °C and below were annealed bare. Samples annealed above 600 °C were protected by a 0.3 micrometer layer of silicon dioxide. This layer was deposited in an IPC ion-beam sputtering system. No visible degradation of the GaAs surface was observed after annealing treatments.

Implanted layers were initially characterized by sheet resistance and junction depth measurements. Results are given in Table 1 and Figures 6, 7 and 8. The data of Figure 6 show reverse annealing occuring between room temperature and 450 ° - 550 °C, probably resulting from the breakup of defect complexes formed during implantation. A rapid decrease in sheet resistance occurs at higher temperatures, corresponding to the re-ordering of the lattice and the elimination of defects. Above 650 °C, the sheet resistance decreases slowly with increasing temperature. Each annealing step is 30 minutes.

Optimum values of junction depth were obtained from 600 - 800 keV zinc implants. A maximum sheet resistance of 200 ohms/square was required; this corresponds to a contribution to cell series resistance of 0.15 ohm, using a 14-finger front contact. The data of Figure 7 shows that the required dose is 2×10^{15} ions/cm^2. This corresponds to 25% utilization; i.e., the measured sheet resistance is 4 times greater than calculated using bulk mobility values. This discrepancy may result from incomplete activation of the zinc as an acceptor (e.g., zinc atoms located interstitially or on arsenic sites) or lowered mobility in the implanted layer due to residual radiation damage; probably both effects are present.

Junction depth measurements were made by angle lapping and staining with 1 HNO_3 : 9 H_2O. The photographs in Figure 8 show the excellent junction delineation achieved. The measured junction depths corresponded to those calculated from range-energy theory[7] for all annealing schedules employed, showing that diffusion of the implanted zinc was slight up to 800 °C.

Table 1. Characteristics of Zinc Implants in n-type GaAs.

Implant Energy E (keV)	Dose N (cm^{-2})	Sheet Resistance ρ_S $(\Omega/\square)$	Junction Depth x_j (μm)	Resistivity $\bar{\rho} = \rho_S x_j$	N_A (cm^{-3})
Background Concentration, $N_B = 2 \times 10^{17}$ cm^{-3}					
200	10^{15}	345	0.12 - 0.15	$4.65 \cdot 10^{-3}$	$2.1 \cdot 10^{19}$
	$2 \cdot 10^{15}$	286	0.12 - 0.15	$3.86 \cdot 10^{-3}$	$2.3 \cdot 10^{19}$
400	10^{15}	195	0.3	$5.7 \cdot 10^{-3}$	$1.5 \cdot 10^{19}$
	$2 \cdot 10^{15}$	Sample Lost in Processing			
600	$5 \cdot 10^{14}$	490	0.38	$1.86 \cdot 10^{-2}$	$2.5 \cdot 10^{18}$
	10^{15}	318	0.38	$1.21 \cdot 10^{-2}$	$5 \cdot 10^{18}$
	$2 \cdot 10^{15}$	177	0.38	$6.72 \cdot 10^{-3}$	$1.2 \cdot 10^{19}$
	$5 \cdot 10^{15}$	145	0.44	$6.38 \cdot 10^{-3}$	$1.3 \cdot 10^{19}$
800	$5 \cdot 10^{14}$	453	0.4	$1.81 \cdot 10^{-2}$	$2.5 \cdot 10^{18}$
	10^{15}	308	0.51	$1.57 \cdot 10^{-2}$	$3 \cdot 10^{18}$
	$2 \cdot 10^{15}$	168	0.51	$8.56 \cdot 10^{-3}$	$9 \cdot 10^{18}$
	$5 \cdot 10^{15}$	136	0.64	$8.7 \cdot 10^{-3}$	$8 \cdot 10^{18}$
1000	10^{15}	313	0.63	$1.97 \cdot 10^{-2}$	$2.1 \cdot 10^{18}$
	$2 \cdot 10^{15}$	172	0.70	$1.2 \cdot 10^{-2}$	$5 \cdot 10^{18}$
1200	10^{15}	304	0.76	$2.31 \cdot 10^{-2}$	$1.8 \cdot 10^{18}$
	$2 \cdot 10^{15}$	150	0.82	$1.23 \cdot 10^{-2}$	$5 \cdot 10^{18}$
1400	10^{15}	–	0.88	Sample Lost in Processing	
	$2 \cdot 10^{15}$	168	0.88	$1.48 \cdot 10^{-2}$	$3 \cdot 10^{18}$
Background Concentration, $N_B = 1 \times 10^{16}$ cm^{-3}					
600	10^{15}	170	0.5	$8.5 \cdot 10^{-3}$	10^{19}
	10^{15}	160	0.5	$8.0 \cdot 10^{-3}$	10^{19}
800	10^{15}	81	0.64	$5.2 \cdot 10^{-3}$	$1.7 \cdot 10^{19}$
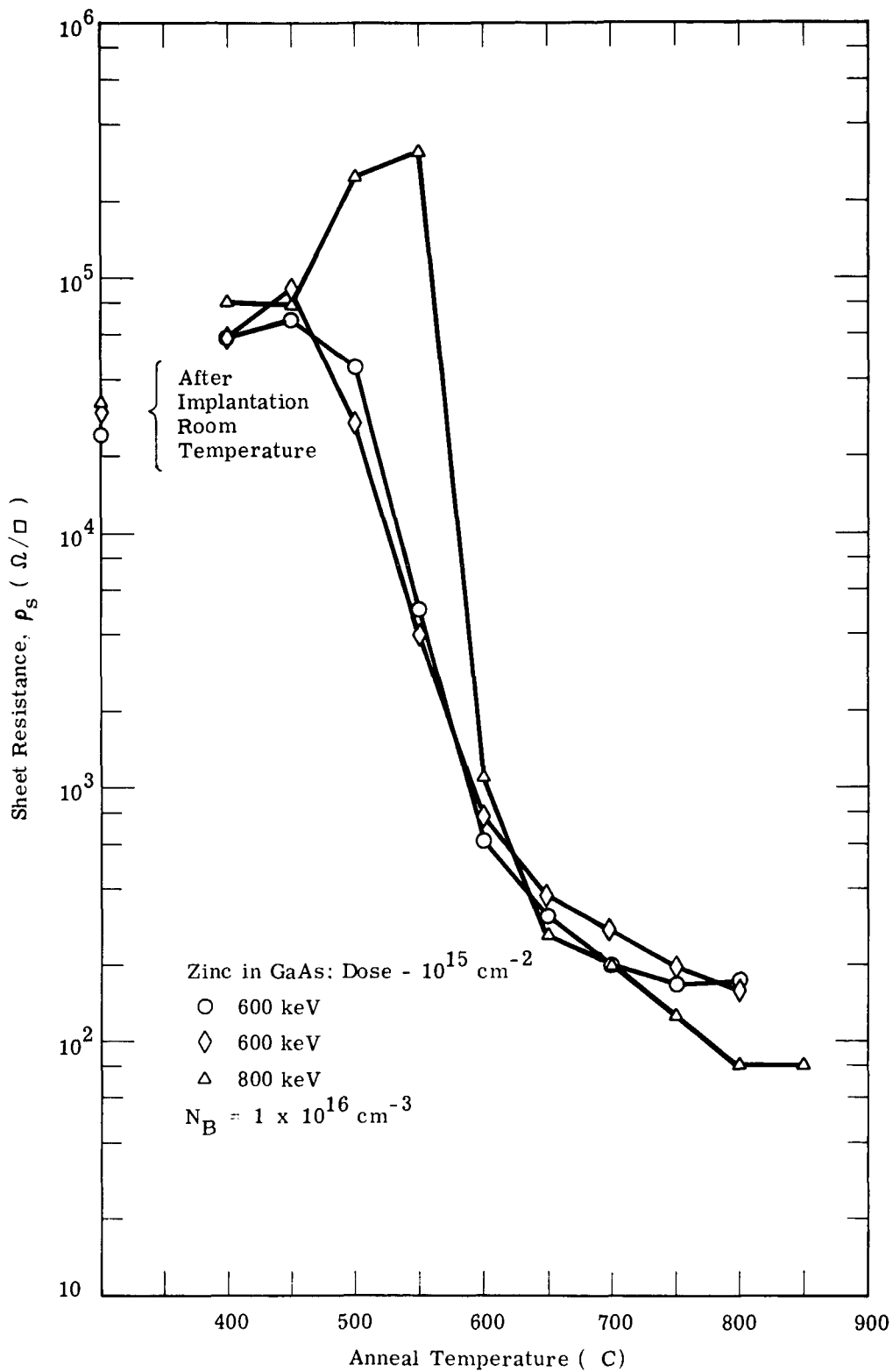
Figure 6. Sheet Resistance versus Annealing Temperature for 600 and 800 keV Zinc in GaAs and 10^{15} cm^{-2} Dose.

1-6360

15

Sheet Resistance, ρ_S ($\Omega \cdot \square$)

10^3

◊ 600 keV 700 °C Anneal
○ 600 keV 750 °C Anneal
△ 800 keV 700 °C Anneal
□ 800 keV 750 °C Anneal

$N_B = 2 \cdot 10^{17}$ cm^{-3}

10^2

10^{14}

10^{15}

10^{16}

Implanted Dose (Zn/cm^2)
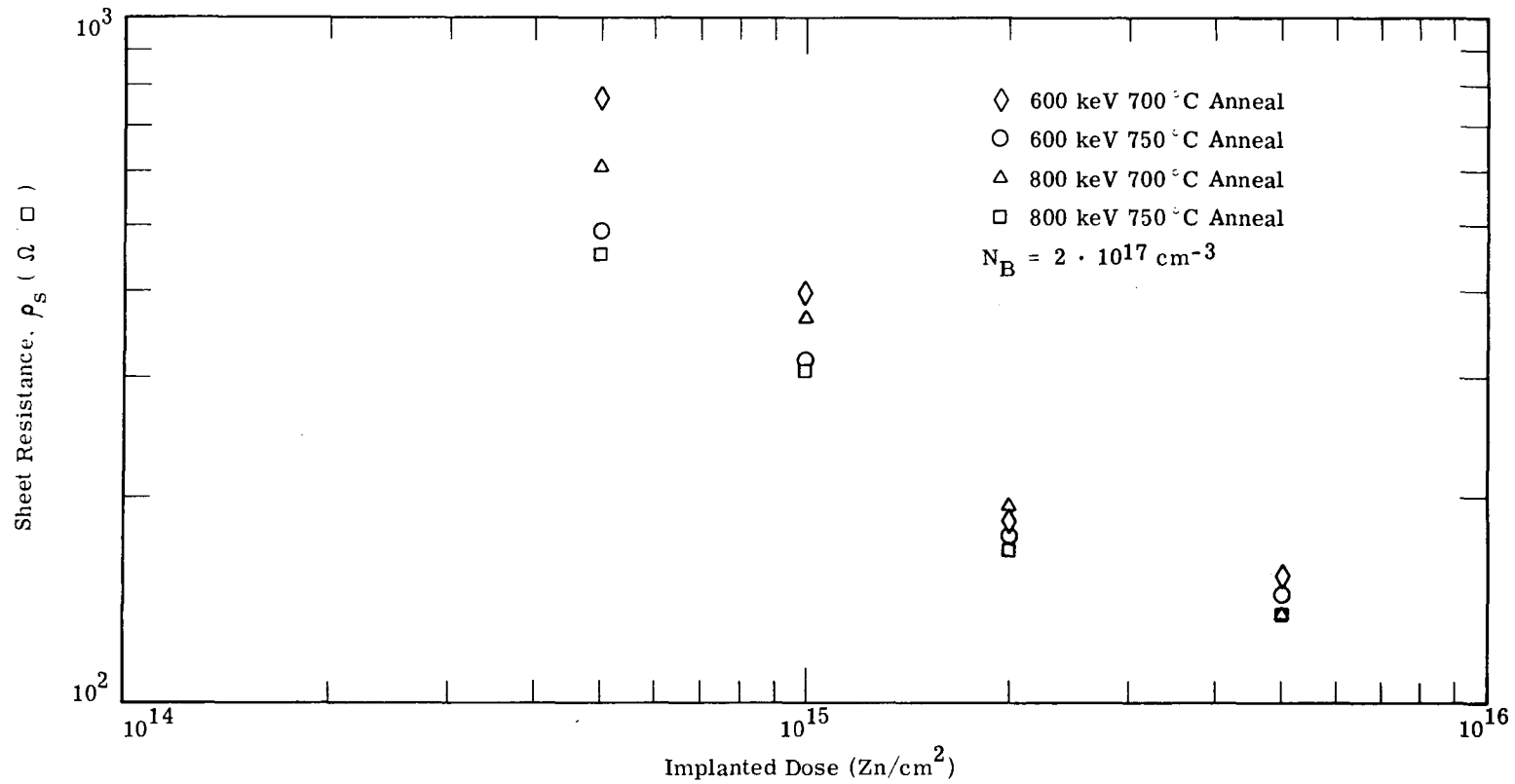
Figure 7.   Sheet Resistance versus Implanted Dose for 600 and 800 keV
Zinc in GaAs at Two Anneal Temperatures.
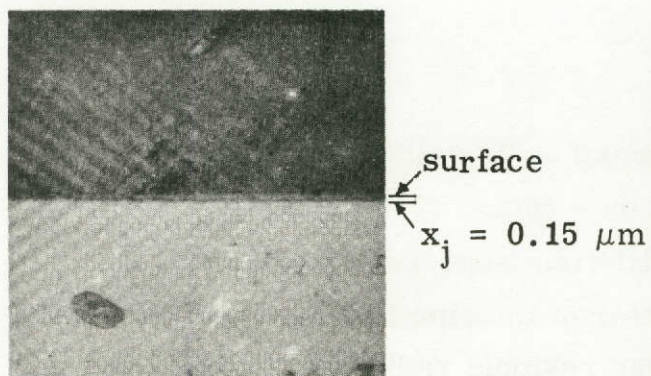
a. 200 keV; 10^{15} cm^{-2}
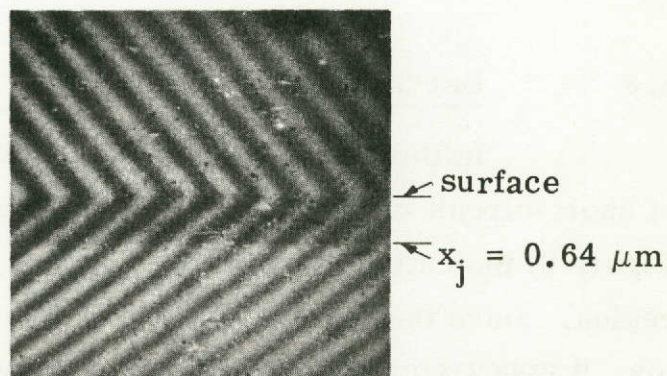
surface
$x_j = 0.15$ μm

d. 800 keV; $5 \cdot 10^{15}$ cm^{-2}

surface
$x_j = 0.64$ μm

b. 600 keV; 10^{15} cm^{-2}

surface
$x_j = 0.38$ μm

e. 1.0 MeV; 10^{15} cm^{-2}

surface
$x_j = 0.63$ μm

c. 800 keV; $2 \cdot 10^{15}$ cm^{-2}

surface
$x_j = 0.51$ μm

f. 1.4 MeV; 10^{15} cm^{-2}

surface
$x_j = 0.88$ μm
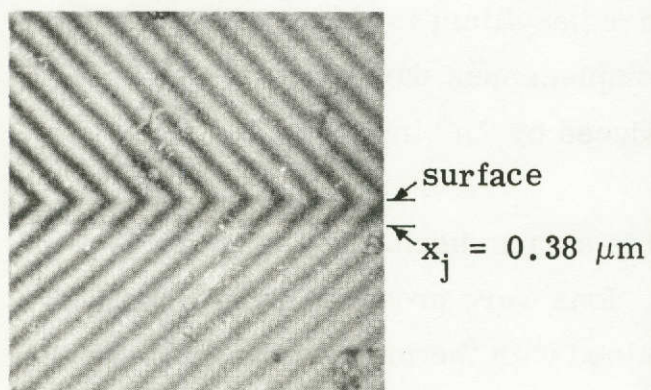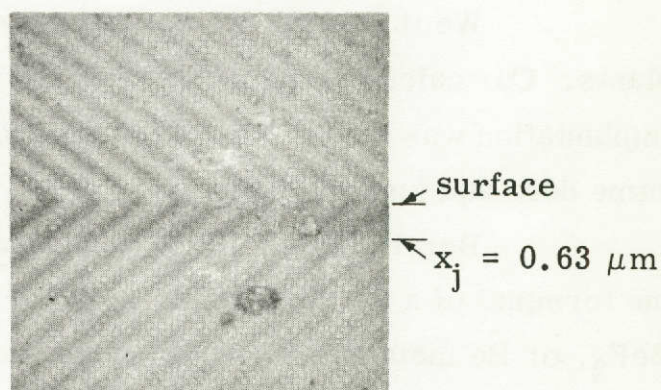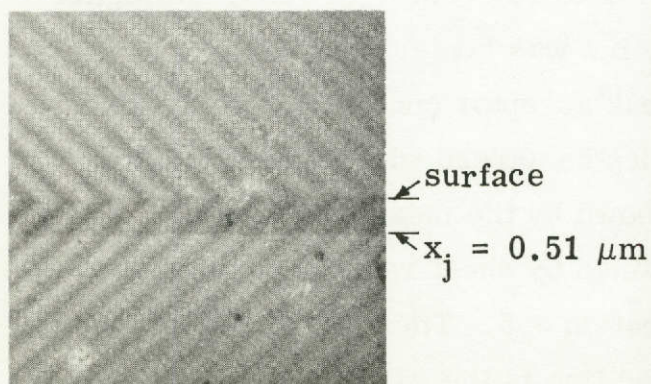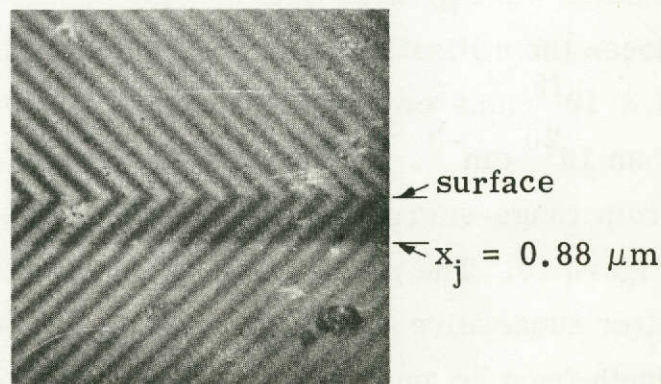
Figure 8.   Photographs of Junction Delineation in GaAs
for Several Implant Conditions.

2-1614

17

3.3 Beryllium Implantation

Initial evaluation of zinc-implanted solar cells showed a severe loss of short-circuit current, especially in the blue region of the spectrum (see Figure 9) indicating low minority carrier lifetime especially in the surface region. Since the measured utilization factor of the zinc implants was relatively low, it appeared possible than the cause was residual radiation damage. An article[8] appearing at about this time reported that Be^+ and Mg^+ ions implanted in GaAs produced P-type layers. The Be^+ implanted layers exhibited high (>80%) utilization factors after low (600 °C) temperature annealing.

We therefore decided to compare beryllium implants with zinc implants. Our calculations showed that the displacement damage produced by Be^+ implantation was only about 3% of that produced by Zn^+ implantation, for the same dose and junction depth.

Beryllium ions were produced in an arc discharge source located in the terminal of a 300 keV ion accelerator. Ions were produced from $BeCl_2$, BeF_2, or Be metal; best results were obtained with the metal. Fairly large ion currents (about 10 μA) could be easily obtained, but source stability was best when lower currents (2.0 to 2.5 μA) were drawn.

Results of beryllium implants are given in Table 2. Utilization factors were greater than 80% for doses of 1 x 10^{15} cm^{-2} or less. At higher doses the utilization factor fell somewhat, but was larger than 50% at 5 x 10^{15} ions/cm^2, corresponding to a peak acceptor concentration greater than 10^{20} cm^{-3}. The measured junction depths agreed with those calculated from range-energy theory (Table 3), as shown by the measurements in Figure 10. The points (circles) were obtained by sheet resistance measurements after successive etches as described in Section 3.5. The triangle is the junction depth from an angle section, and the dashed line is the calculated doping profile.

3.4 Contacts

Initially, electrical contacts were applied by vacuum evaporation of a silver-indium alloy (25% In) from a tungsten filament on substrates heated to

Table 2. Characteristics of Be^+ Implants

E(keV)	Dose (cm^{-2})	Ann (°C)	R_S (Ω/□)	x_j (μm)	Co/A (nf/cm^2)	$n^{(1)}$	$A^{(2)}$
40	10^{15}	700	815	--	57	0.30	2.2
70	10^{15}	700	158	0.48	83	0.45	2.2
100	10^{15}	700	113	0.53	81	0.45	2.2
		775	95	0.60	90	0.48	2.2
		850	190	0.75	--	--	--
	5×10^{14}	700	265	0.50	--	--	--
		775	(3)	0.50	--	--	--
		850	(3)	0.50	--	--	--
	10^{14}	700	500	0.35	--	--	--
		775	405	0.35	--	--	--
		850	885	0.50	--	--	--
200	10^{15}	775	120	0.75	--	--	--
	5×10^{15}	775	39	0.95	--	--	--
	9×10^{15}	775	31	0.95	--	--	--

NOTES: All implants into 2×10^{17} cm^{-3} T_e-doped N-type material.

[1] Obtained from C-V measurements: $C \propto (V + V_o)^{-n}$

[2] Obtained from dark I-V measurements ($V_F < 0.9$ volt): $I \propto \exp (qV/AkT)$.

[3] High sheet resistance resulting from failure of sputtered silica protective coating. Other 850 °C results are also affected.

Table 3. Projected Range and Standard Deviation of Projected Range for Be$^+$ in GaAs.

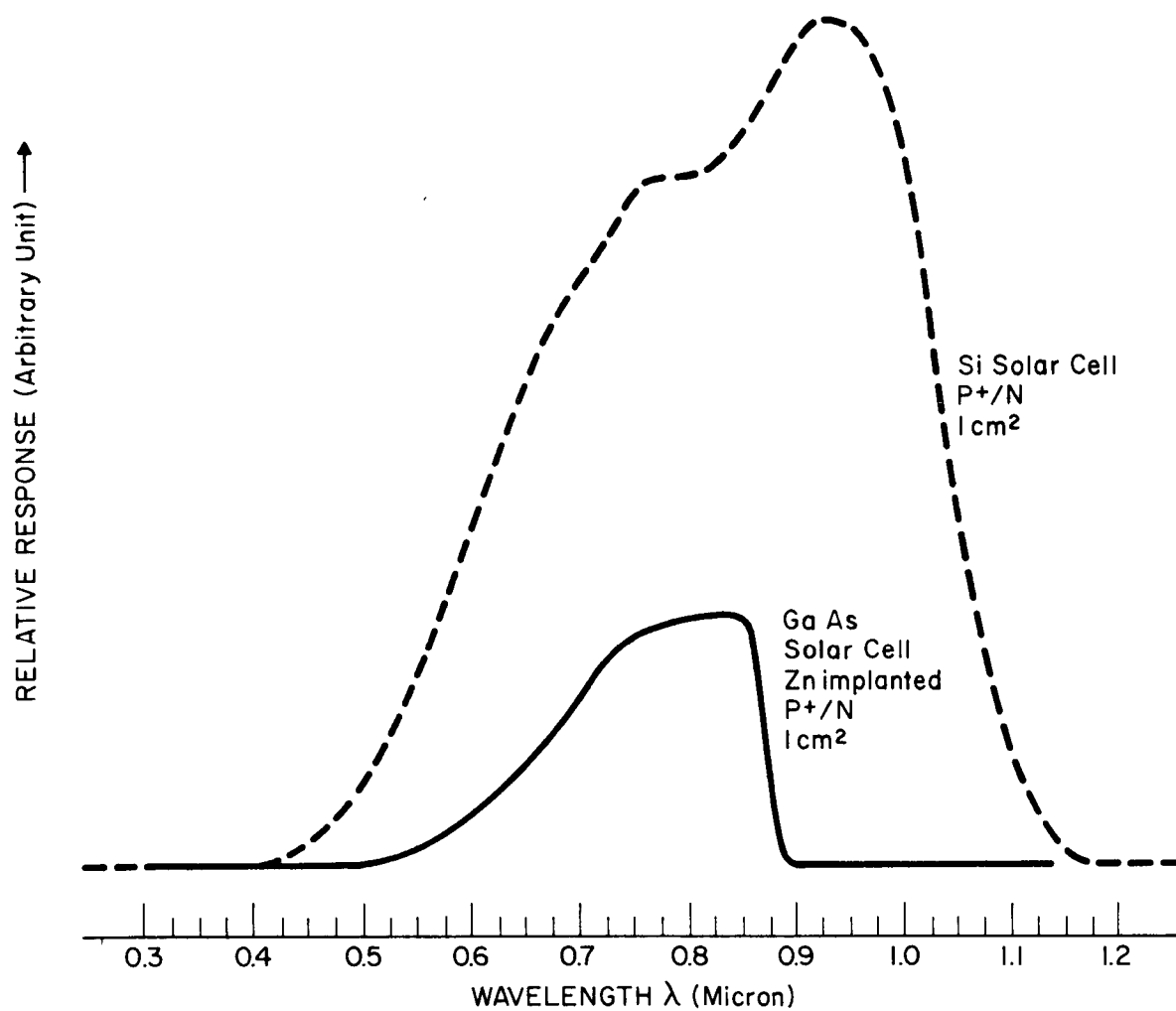| E, keV	R_p, μm	σ, μm
40	0.1106	0.0550
50	0.1392	0.0645
60	0.1680	0.0732
70	0.1969	0.0811
80	0.2255	0.0883
90	0.2538	0.0949
100	0.2821	0.1012
110	0.3105	0.1070
120	0.3387	0.1124
130	0.3669	0.1174
140	0.3948	0.1221
150	0.4224	0.1265
160	0.4497	0.1306
170	0.4766	0.1345
180	0.5029	0.1381
190	0.5287	0.1416
200	0.5539	0.1449

Figure 9. Relative Spectral Response of Zn⁺ Implanted
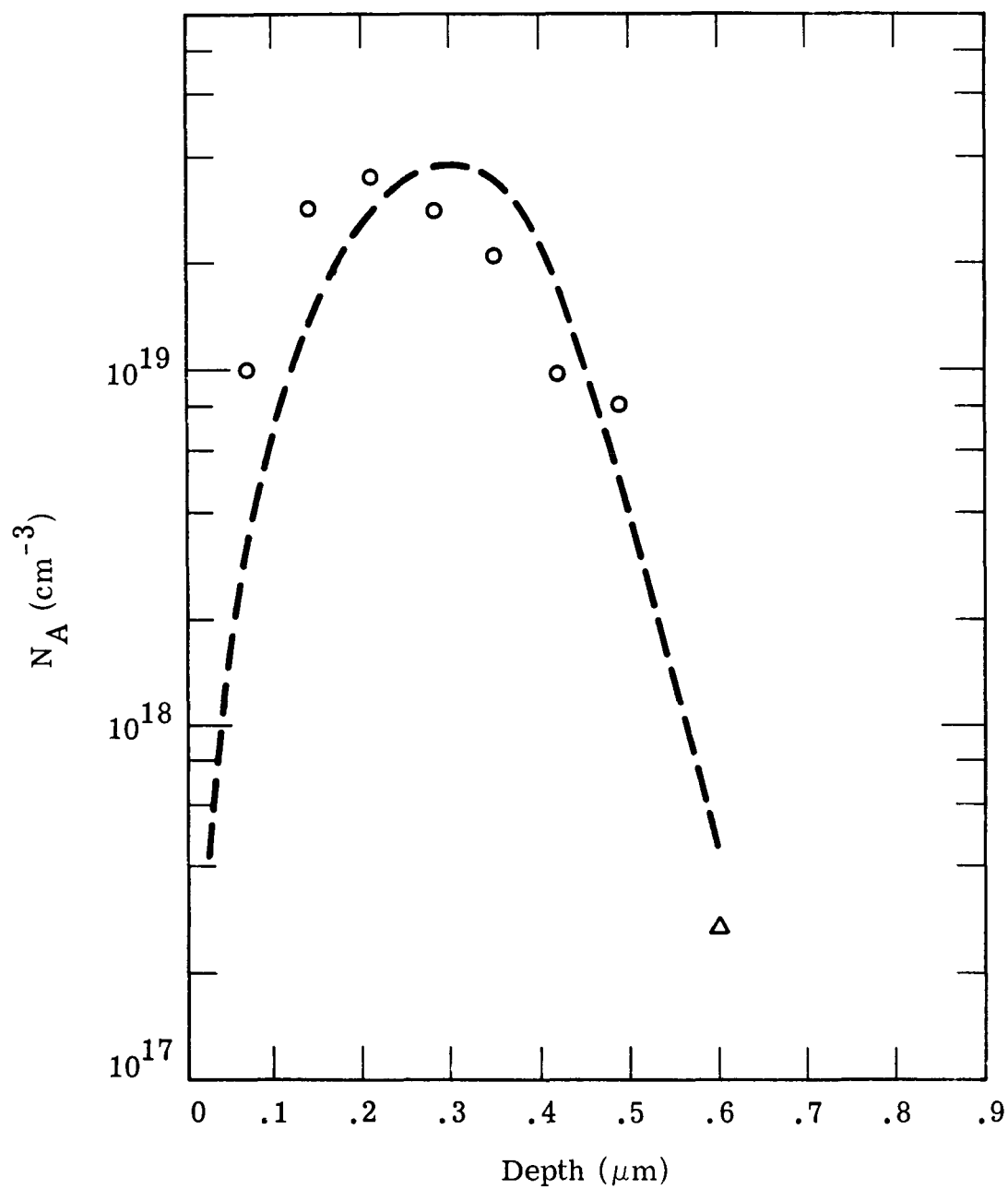GaAs Solar Cell

Figure 10.   Profile of Implanted Be in GaAs (100 keV, 10^{15} cm^{-2}, annealed 775 °C, 20 minutes).

1-6418

22

300 °C. After deposition, contacts showed fair adherence and the specific contact resistance was measured to be 2×10^{-2} ohm-cm^2. Firing in hydrogen at 500 °C for 10 minutes improved adherence and reduced the specific contact resistance to 9×10^{-4} ohm-cm^2. These contacts were adequate for experimental purposes but were not sufficiently reproducible to be entirely satisfactory.

An improved process was developed which produced extremely adherent, low-resistance contacts. These contacts not only withstand the usual tape and abrasion tests, but also vigorous abrasion with metal tweezers without peeling. Interconnection is possible either by soldering or ultrasonic welding.

The improved process is as follows:

(1)   Etch sample in 1 H_2SO_4 : 1 H_2O_2 : 100 H_2O for 15 seconds immediately prior to contact evaporation. The amount of material removed in the etch is small (< 0.1 micrometer).

(2)   Heat the sample to 300 °C in the evaporator. Evaporate a thin (sub-micron) layer of indium and zinc on the front (implanted) surface. The source is a tungsten filament wound with indium wire to which a few clips of zinc wire are added. The filament is pre-wet before evaporating by heating in the evaporator with the shutter closed.

(3)   Immediately follow with a thicker layer of pure silver.

(4)   Contact the backs of the samples in the same way, adding tin instead of zinc to the indium evaporation.

(5)   Fire in hydrogen. Initially a temperature of 560 °C was used; some samples showed low shunt resistance after firing, indicating penetration of metallization through the junction in isolated areas. The firing temperature was reduced to 450 °C for later samples to eliminate this problem.

Since the substrate temperature during both evaporation and firing is well above the melting point of indium, this is actually an alloyed contact. Because of the low temperature and small amount of liquid phase present, the alloying can be controlled to give an adherent low-resistance contact without junction penetration. Further development should eliminate the firing step. Metal masks were used; although the indium layer is liquid, no spreading of the layer under the mask was observed.

3.5 Post-Contact Etching

A slow etch is needed in GaAs cell fabrication for the following purposes:

(1) Clean-up prior to contact deposition.

(2) Profiling of implanted layers, as in Figure 10.

(3) Removal of material to bring the peak of the implanted profile to the surface, as discussed in Section 4.2.

The etch composition 1 H_2SO_4 : 1 H_2O_2 : 100 H_2O was found to be satisfactory for these purposes. It does not attack the contact metallization, and so can be used after metallization. When used for the second and third purposes mentioned above, the sample is dipped into the etchant (at room temperature) for successive 15-second etches. After each step the sample is rinsed in de-ionized water. The amount of material removed from the implanted face of the sample was measured to be .07 ± .01 micrometers per 15-second etch step, by interferometry using the metallized contact surface as a reference.

After several etching steps, a partially opaque film appears to build up on the etched surface. This film has been noticed by others[9] and found to be composed of As_2O_3. Since As_2O_3 is more readily soluble in basic than acidic aqueous solutions, we etched another sample in a slow NaOH : H_2O_2 etch; the film was less evident but the etch was also less controllable. We believe that a satisfactory procedure for eliminating film formation would be to rinse the sample in a mildly basic solution for several minutes after each etching step, but we did not verify this procedure by further experiment.

SECTION 4
ELECTRICAL MEASUREMENTS

4.1   Dark Measurements

Capacitance-voltage measurements were made on small area diodes fabricated by mesa etching, over the voltage range 0 to -4 volts. Results on both zinc-implanted and beryllium-implanted samples conformed closely to the expected behavior of an abrupt P^+N diode. These measurements indicated the absence of a compensated region at the junction. This conclusion was further confirmed by the fact that the reverse breakdown voltage of these diodes agreed closely with the value calculated for an abrupt junction.

Measurements of forward current density as a function of applied voltage were made; typical results are shown in Figure 11, which shows measurements made on the four quarters of a 2 x 2 cm Be^+-implanted (100 keV, 10^{15} cm^{-2}, annealed 700 °C, 20 min.) solar cell. The samples are shown in Figure 12. The two quarters containing the contact bar show a low shunt resistance, attributed to penetration of the junction by the contact metallization in localized areas. This sample had the contacts fired at 560 °C; for subsequent samples, the firing temperature was reduced to 450 °C with noticeable improvement in shunt resistance.

The best quarter of the cell (sample 4) exhibits a dark forward characteristic which conforms closely to the behavior expected of a PN junction dominated by space-charge recombination:

$$ J = \frac{q \, n_i \, w}{2\tau} \quad \exp \quad \frac{qV}{2kT} $$

The width of the space-charge region is known from the C-V measurements ($w = 10^{-5}$ cm); the data of sample 4 therefore yields a value for the effective lifetime in the space-charge region. This value is 2.6×10^{-8} seconds, which
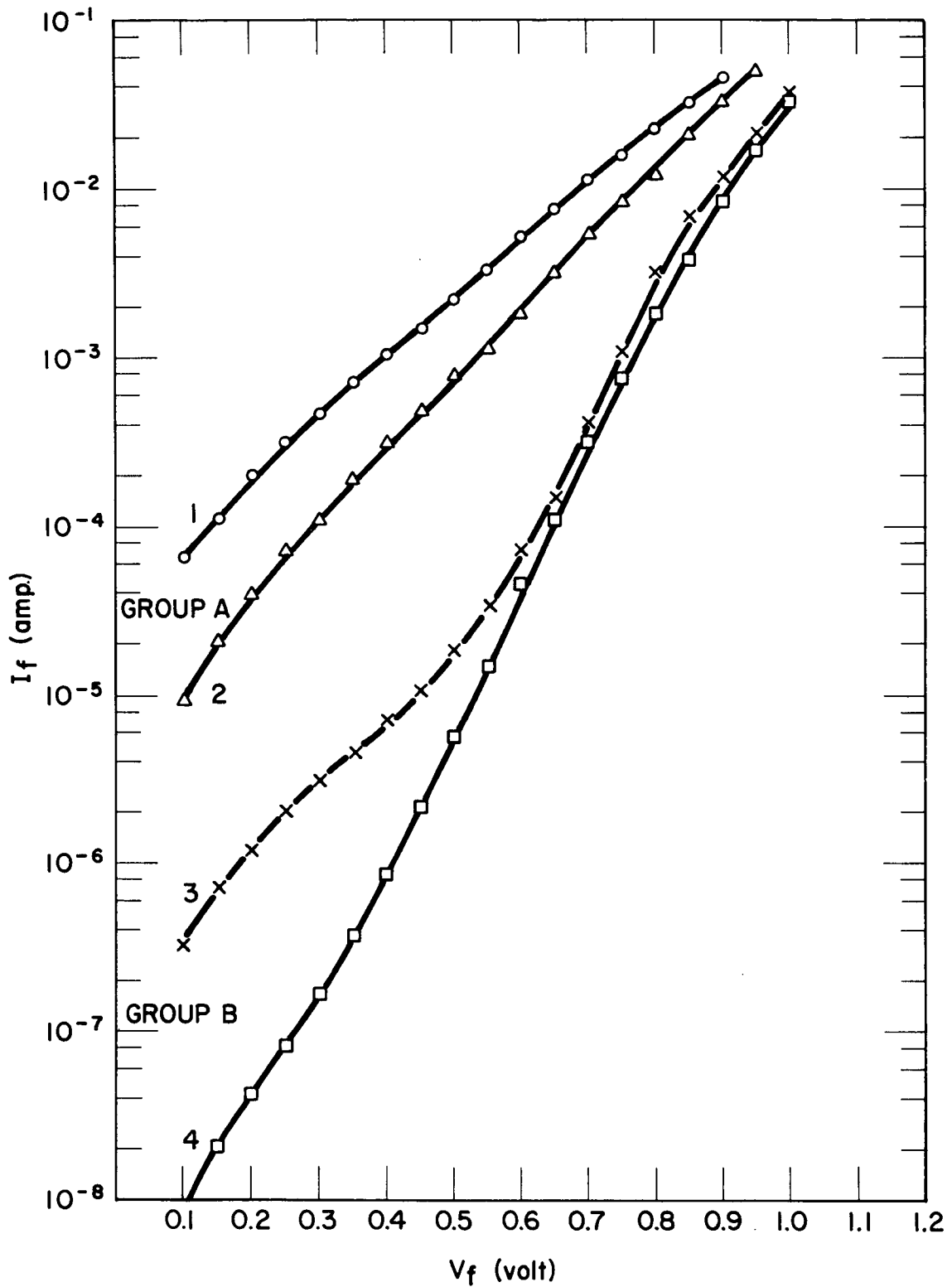
25

Figure 11. Dark Forward I-V Characteristics of a Be^+ Implanted (100 keV, 10^{15} cm^{-2}) P^+N Solar Cell (4 cm^2) Scribed into Four Small Samples
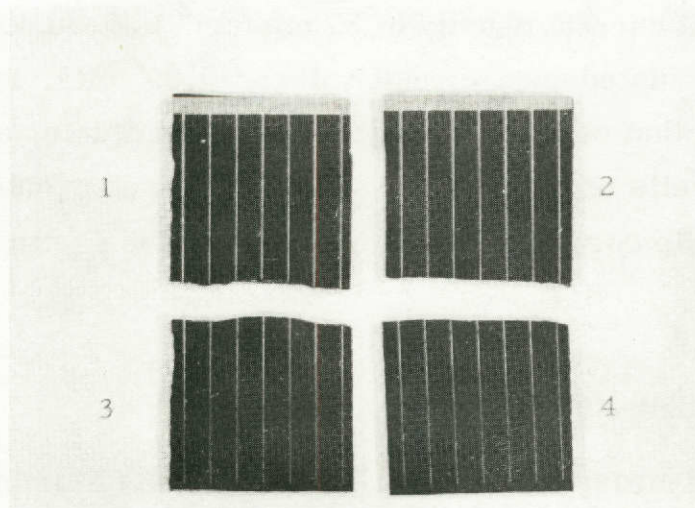
1-6416

Figure 12.   A Be$^+$ Implanted (100 keV, 10^{15} cm^{-2}) P$^+$N
Solar Cell (4 cm^2) Scribed Into Four Small
Samples. Cell #1 and #2 (Group A) Have
Larger Contact Area Than Cell #3 and #4
(Group B).

agrees closely with the sum of the hole and electron minority carrier lifetimes $(1.9 \times 10^{-8}$ seconds) assumed in the theoretical calculations (Figures 2 and 3). We can therefore conclude that our fabrication process has preserved the minority carrier lifetime in the base material. Also, the forward voltage at the calculated short-circuit current density of 35 mA/cm^2 is 0.98 volts, in close agreement with the calculated open-circuit voltage (0.99 volts, Figure 4). We can therefore conclude that cell series resistance is negligible, and our beryllium-implanted solar cells (except for the shunt resistance problem discussed above) conform closely to our calculations insofar as base lifetime and junction quality are concerned.

4.2   Illuminated Measurements

Illuminated measurements were made in AMO illumination (140 mW/cm^2) provided by a carbon arc solar simulator standardized by comparison with a silicon solar cell calibrated against a JPL balloon-flight standard cell. Additional measurements of cell spectral response were obtained using a tungsten light source with a Bausch and Lomb grating monochromator.

In the AMO measurements (Table 4), the short-circuit current values measured under AMO illumination were found to be very low, typically about 5 mA/cm^2. Since these cells did not have an anti-reflecting coating, the anticipated value of short-circuit current (corresponding to the computed short-circuit current of 35 mA/cm^2 in a completed cell) was 25 mA/cm^2.

We initially attributed the low values of J_{sc} to the presence of a "dead layer" in these cells, arising from the fact that the doping profile produced by implantation results in a region between the surface and the peak of the implanted distribution in which the impurity gradient produces an electric field which causes minority carriers to drift towards the surface instead of towards the junction. As can be seen from Figure 10, the thickness of this region is approximately 0.2 micrometers for cells implanted with beryllium at 100 keV to 10^{15} cm^{-2}.

Table 4. Characteristics of Solar Cells.

Impl. and Ann. Parameters[1]	x_j, μm	J_{sc}, mA/cm^2	V_{oc}	CF[2]
Zn^+ Implants:				
800, 2 x 10^{15}, 700, 30	0.50	5.63	0.605	0.63
800, 2 x 10^{15}, 700, 30	0.50	4.70	0.578	0.62
600, 5 x 10^{15}, 700, 30	0.45	4.12	0.580	0.56
800, 2 x 10^{15}, 650, 180	0.45	2.14	0.550	0.65
800, 2 x 10^{15}, 650, 180	0.45	2.45	0.545	0.50
800, 5 x 10^{15}, 650, 180	0.50	3.05	0.476	0.46
800, 2 x 10^{15}, 800, 30	0.55	5.00	0.520	0.39
800, 2 x 10^{15}, 800, 30	0.60	4.30	0.490	0.42
600, 5 x 10^{15}, 800, 30	0.55	3.67	0.605	0.55
Be^+ Implants:				
40, 1 x 10^{15}, 700, 20	0.30	6.37	0.530	0.61
70, 1 x 10^{15}, 700, 20	0.45	6.47	0.672	0.59
100, 1 x 10^{15}, 700, 20[3]	0.53	4.84	0.538	0.48
100, 1 x 10^{15}, 700, 20[3]	0.53	5.00	0.660	0.58
100, 1 x 10^{15}, 700, 20[3]	0.53	5.05	0.796	0.75
100, 1 x 10^{15}, 700, 20[3]	0.53	5.14	0.810	0.79
200, 1 x 10^{15}, 775, 20	0.75	2.67	0.660	0.71
200, 9 x 10^{15}, 775, 20	0.95	4.38	0.700	0.59
Be^+ Implants, Etched:				
100, 1 x 10^{15}, 775, 20	0.11[4]	11.0	0.820	--
200, 1 x 10^{15}, 775, 20	0.30[4]	10.0	0.730	0.79

NOTES: All implants into 2 x 10^{17} cm^{-3} Te-doped N-type material. No anti-reflective coating applied.

[1] Parameters are: implantation energy (keV), dose (ions/cm^2), annealing temperature (°C) and time (minutes).

[2] Curve factor: $I_{mp} V_{mp} / I_{sc} V_{oc}$

[3] Samples 1, 2, 3 and 4; other data in Figures 11 and 12.

[4] After etching 7 times (100 keV sample) and 8 times (200 keV sample) in 1 H_2SO_4 : 1 H_2O_2 : 100 H_2O.

We therefore etched several samples as described in Section 3.5, making spectral response measurements after each 15-second etch. The results for a sample implanted with beryllium at 100 keV, 10^{15} cm^{-2}, annealed at 775 °C, 20 minutes, are given in Figure 13. The numbers on the curves indicate the number of etching steps. The ordinate is proportional to the short-circuit current of the cell, uncorrected for the variation in intensity with wavelength of the source.

Referring again to Figure 10, it can be seen that after three etching steps the peak of the implanted distribution will lie at the surface. The doping gradient between this point at the junction is sufficiently great so that the minority carriers (electrons) will experience a field sufficiently large to cause them to drift with maximum velocity (10^7 cm/sec). Under these circumstances, surface recombination will be small for all possible values of surface recombination velocity, as discussed in Section 2. Therefore, we would expect to see a substantial improvement after three etching steps and little improvement thereafter, if surface recombination were the major cause of low J_{sc} in unetched samples. Instead, as can be seen from Figure 13, the sample continue to improve with further etching. After 7 etching steps, the junction depth has been reduced to about 0.1 micrometers and the short-circuit current has improved to 11 mA/cm^2, still more than a factor of two below the expected value. Part of this discrepancy results from the presence of an absorbing film of As$_2$O$_3$, as discussed in Section 3.5.

4.3   Analysis of Etching Experiments

The data of Figure 13 can be further analyzed to extract information on the minority carrier diffusion lengths in the surface and bulk regions of the solar cell. Consider a solar cell exposed to a flux of H photons/cm^2-sec of monochromatic light. The carrier generation rate in an element of thickness dx is

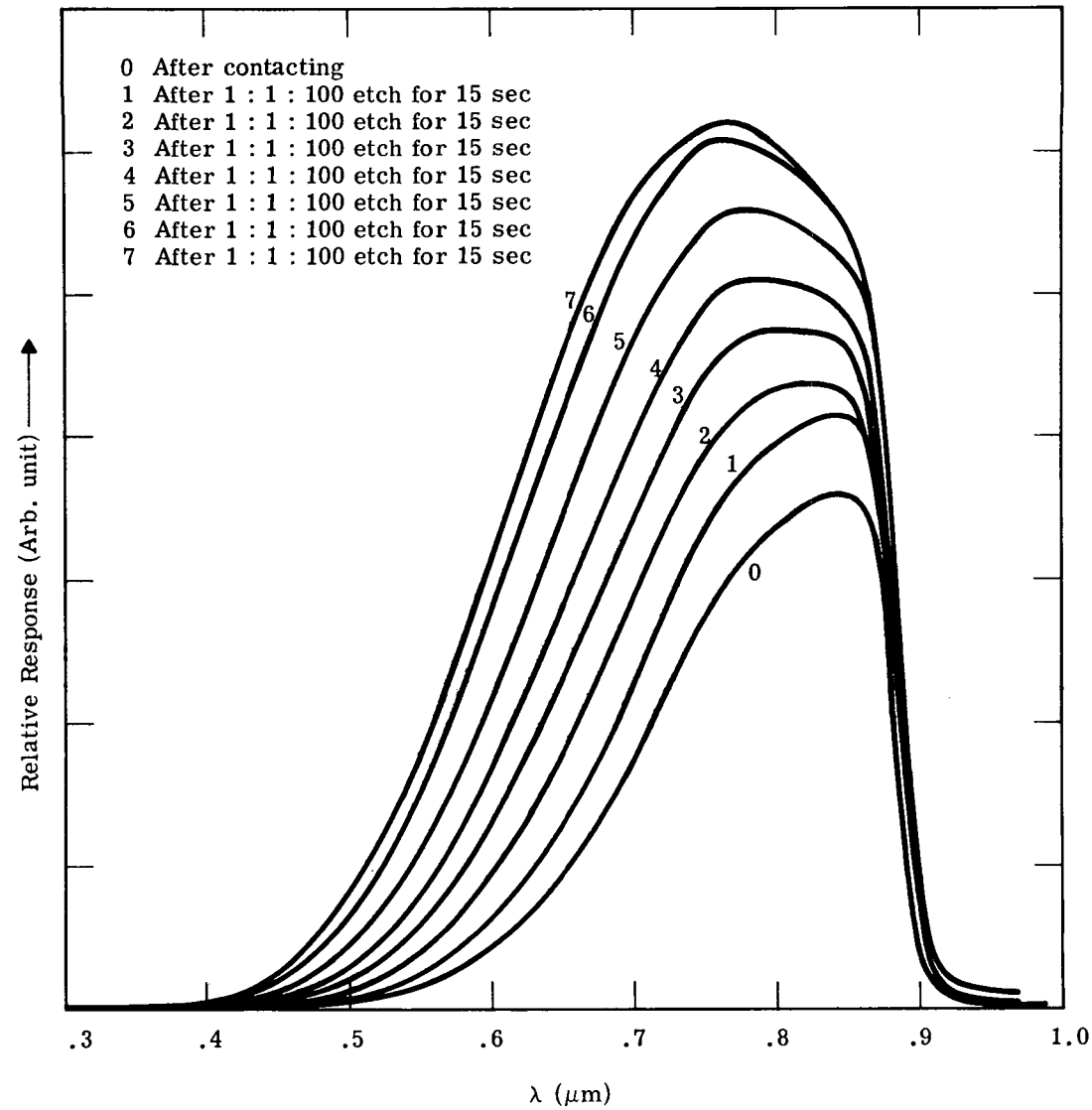$$G = H(1 - R) \propto \exp(-\propto x)\, dx$$

Figure 13.   Spectral Response of Etched Be-Implanted GaAs Solar Cell (100 keV, 10^{15} cm^{-2}, annealed 775 °C, 20 minutes, etched 15 seconds per step).

where

$$R \;=\; \text{reflectivity}$$

$$\propto \;=\; \text{absorption coefficient}$$

The short-circuit current density can be expressed as:

$$J_{sc} \;=\; \int_{0}^{\infty} qG \exp - (d - x)/L_s \;+\; \int_{d}^{\infty} qG \exp -x/L_b$$

The two integrals are the contribution to J_{sc} from the surface and bulk regions, respectively, and L_s and L_b are the minority carrier diffusion lengths in these regions. The junction depth is d, and it is assumed that the junction depletion layer thickness is negligible and the cell is infinitely thick. Performing the integrations yields:

$$\frac{J_{sc}}{qH(1-R)} \;=\; \frac{\propto L_s}{1-\propto L_s} \left[\exp(-\propto d) - \exp\left(-\frac{d}{L_s} \right) \right] \;+$$

$$\frac{\propto L_b}{1 + \propto L_b} \exp\left(-\propto d - \frac{d}{L_b} \right)$$

The above calculation assumes that L_s and L_b are constants independent of position in the device. This is a good assumption with respect to L_b, but not L_s. The effective value of L_s will depend on d not only because of the variation in doping within the surface layer, but also because of the varying effects of surface recombination and built-in drift fields resulting from doping gradients.

If L_s is assumed to be zero:

$$\frac{J_{sc}}{qH(1-R)} \;=\; \frac{\propto L_b}{1 + L_b} \exp\left(-\propto d - \frac{d}{L_b} \right)$$

A semi-log plot of log I_{sc} against d will then be a straight line of slope $-(\alpha + 1/L_b)$. For our samples, the effective diffusion length between the (original) surface and the peak of the implanted distribution would be expected to be zero, since the built-in field produced by the doping gradient in this region causes minority carriers to flow towards the surface. Thus we should be able to determine L_b from the slope of that part of a log I_{sc} versus d plot corresponding to values of d between the original surface and the peak of the implanted distribution. Such plots were constructed for several wavelengths between 0.5 and 0.8 microns. In each case these points were found to be on a straight line with a slope slightly more negative than the corresponding value of α at that wavelength as given by Sturge.[1] From these measurements, L_b was determined to be 2.5 ± 1.5 microns.

Figure 14 shows the experimental points for a wavelength of 0.633 microns. The straight line drawn through the points for zero, one, two and three etching steps corresponds to L_b = 1.6 microns, or αL_b = 7 at this wavelength. Also shown in the plot are the calculated curves for αL_s equals 0, 1, 7, and infinity. It can be seen that αL_s is much less than unity (α^{-1} = 0.227 microns at 0.633 microns). While the measured value of L_b corresponds well with the values assumed for the theoretical calculations, the present measurements of L_s yield values one to two orders of magnitude below those reported in the literature and assumed in the calculations of Section 2.

It will be noticed that the points for the last three etching steps fall below the line for αL_s = 0. This is attributed to the build-up of an As_2O_3 film on the sample surface, which was evident upon microscopic examination.

4.4   Possible Causes of Low L_S

The measured values of L_s imply the existence of a very high concentration of recombination centers in the surface region; in fact, the concentration of these centers cannot be too far below the acceptor concentrations in these samples (i.e., of the order of 10^{18} cm^{-3}). The facts that we do not observe a compensated region at the junction and the base region lifetime is in the expected range, suggest that the recombination center is a deep donor,

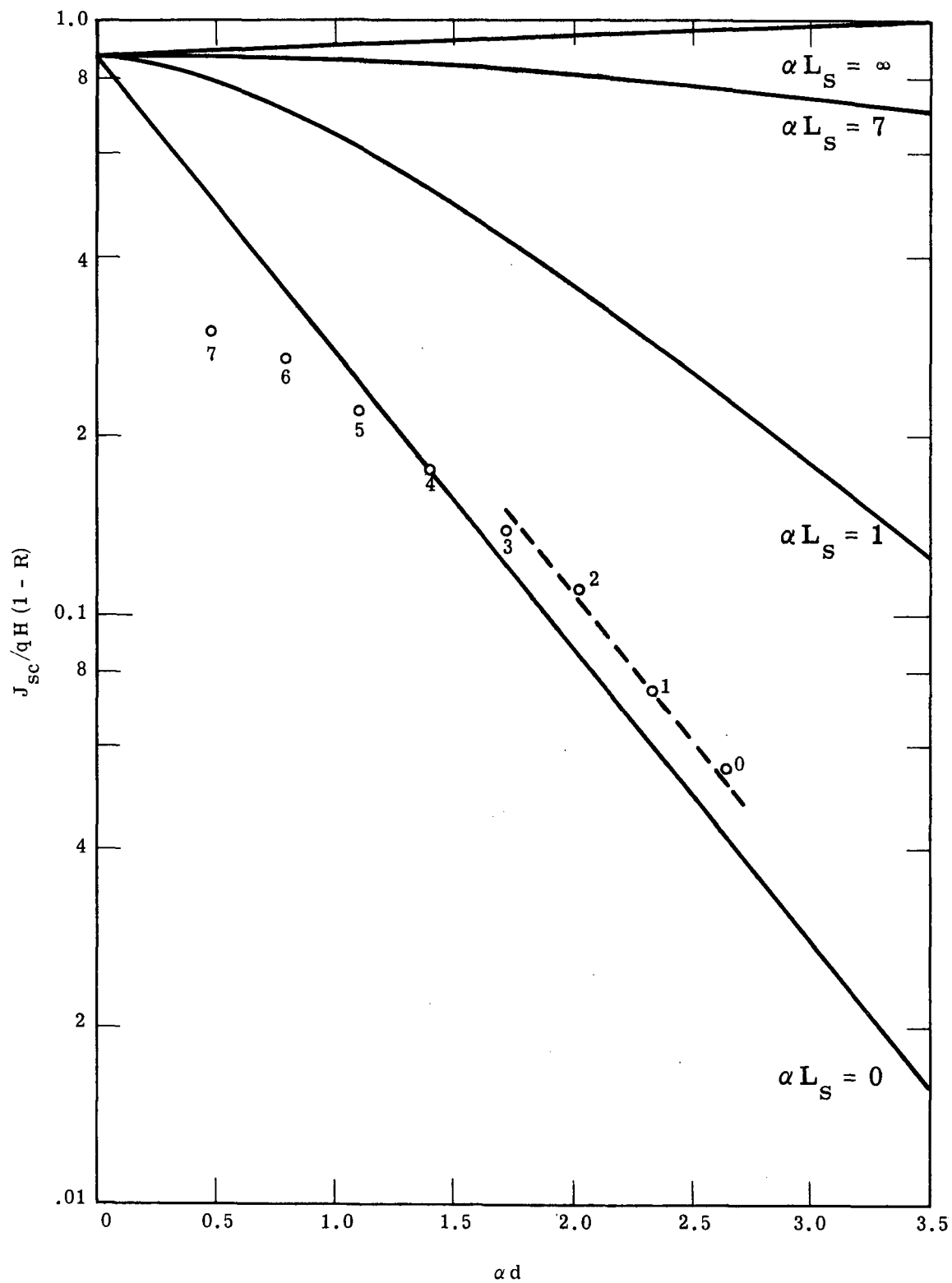Figure 14. Normalized Short Circuit Current Density versus Junction Depth (Illumination at 633 nm; $\alpha = 4.4 \times 10^4$ cm^{-1}; Data Points from Figure 13; Calculated lines are for α L$_s$ Values of 0, 1, 7 and ∞).

1-6420

34

which would be electrically neutral in the N-type base region but positively charged in the P-type surface region, and consequently would be an effective electron trap. It does not seem likely that these recombination centers can be attributed to unannealed radiation damage, in view of the high utilization factor and mobility measured in beryllium-implanted samples. We have therefore searched the literature to find references to impurities in GaAs which might be responsible for the extremely low electron diffusion length in our samples.

The only deep donor for which we could find data is oxygen, although gallium vacancies might also be expected to be donors (by analogy with arsenic vacancies, which are acceptors). Oxygen produces a donor level slightly below mid-band, 0.63 volts above the valence band.[3] Oxygen is found to be present very high concentrations in boat-grown crystals (10^{18} cm^{-3})[10] and even higher concentrations in Czochralski crystals grown with boron oxide encapsulation (10^{19} - 10^{20} cm^{-3})[11] although it appears to be electrically inactive. Its behavior therefore is analogous to its behavior in silicon, in which most of the oxygen is present in the form of electrically inactive precipitates.

Electrically active oxygen might be present in our samples from three sources:

(1) Activation of dissolved, inactive oxygen by reaction with vacancies introduced by beryllium implantation;

(2) Diffusion of oxygen into the sample during annealing, from an absorbed layer (since the surface region is only ~0.5 microns thick, a concentration of 10^{18} cm^{-3} requires only 5×10^{13} cm^{-2} or .05 monolayer);

(3) Diffusion of oxygen into the sample during annealing, from water vapor in the forming gas atmosphere.

The diffusion coefficient of oxygen in GaAs has been measured[11] to be about 10^{-8} cm^2/sec at 775 °C, so that substantial in-diffusion is possible during annealing; hence all three of the mechanisms listed above are plausible sources. In our samples, a sputtered coating of silicon dioxide is applied for protection during annealing. However, this coating is not impervious to water

vapor, and the forming gas used as an atmosphere during annealing does not have an extremely low dew point. In any case, we know that some decomposition of the silica target occurs during sputtering and therefore the surface of the GaAs sample is exposed to energetic oxygen atoms as well as silica molecules during sputtering.

Since oxygen has such a high diffusion coefficient, it should be possible to extract oxygen from GaAs by using a suitable gettering technique, by analogy to the gettering of gold from silicon. We note with great interest that Vilms and Garrett[12] have reported that oxygen is gettered from boat-grown substrate material into a gallium melt during liquid-phase epitaxial growth at 700 °C. By prolonged extraction the oxygen content can be lowered to about 10^{14} cm^{-3}, provided that the atmosphere is entirely free of water vapor. The oxygen appears to diffuse into the gallium melt and to be removed in the flowing hydrogen atmosphere as Ga_2O. The presence of aluminum in the melt should increase the gettering efficiency (since oxygen entering the melt would be immediately precipitated as Al_2O_3), and it is interesting to speculate that the higher efficiency of GaAlAs-GaAs cells fabricated by liquid-phase epitaxy[13] may be due primarily to the removal of oxygen during the epitaxial growth process rather than to the heterojunction structure.

Oxygen-free gallium arsenide is not commercially available, and liquid-phase gettering of implanted samples is not feasible because the solubility of GaAs in liquid metals is too high. It appears that solid-phase gettering into an evaporated film of aluminum might be successful. The annealing process would have to be carried out below the melting point of aluminum (660 °C), but since our earlier work showed that beryllium-implanted layers can be completely annealed at 600 ° - 650 °C, a suitable annealing schedule should be found. Obviously, every effort should be made to eliminate oxygen from the annealing atmosphere; annealing in vacuum seems best. The presence of an aluminum coating on the sample during annealing might also be beneficial in another way: some indiffusion of aluminum might occur, increasing the band gap near the surface and further reducing the effect of surface recombination by adding to the internal field opposing electron motion towards the surface. Therefore the

aluminum layer should be applied before implantation and its thickness chosen
so that the peak of the implanted distribution is at the aluminum-GaAs interface,
to eliminate the need for etching after annealing.

SECTION 5
CONCLUSIONS AND RECOMMENDATIONS

We believe that the results of our calculations, as summarized in Section 2, are valid, and that it is possible to achieve a conversion efficiency greater than 20% in a practical gallium arsenide solar cell. We also believe that, as a result of the work on fabrication techniques summarized in Section 3, we have arrived at a practical fabrication process to produce the structure which our calculations predict will give optimum efficiency. Nevertheless, the cells produced during this program have exhibited disappointly low efficiency, more than a factor of 2 below predicted values even after making allowance for the lack of an anti-reflective coating on the measured samples.

We attribute this discrepancy to extremely low minority carrier lifetime in the surface region, and we believe the measurements presented in Section 4 rule out surface recombination and residual implantation damage as major causes of this discrepancy. We have tentatively attributed our results to the presence of oxygen in the surface region, and we believe this explanation to be consistent with the known properties of oxygen in gallium arsenide and also with the fact that other investigators have achieved greater success with liquid-phase epitaxy. If this conclusion is correct, it should be possible to develop a suitable gettering process to remove oxygen.

Gallium arsenide has an attractive potential for solar cell development because of its higher potential efficiency, higher temperature capabilities and improved radiation resistance, compared to silicon. Although it is more costly than silicon, the higher values of absorption coefficient and mobility make it much more promising than other semiconductor materials as a potential thin film solar cell. In view of these potential advantages, we recommend that further work be undertaken to clarify the results reported here.

SECTION 6
REFERENCES

1. B. Ellis and T. S. Moss, "Calculated Efficiencies of Practical GaAs and Si Solar Cells Including the Effects of Built-In Fields; Solid-State Electronics 13, 1 (1970).

2. M. D. Sturge, "Optical Absorption of Gallium Arsenide Between 0.6 and 2.75 eV", Phys. Rev. 127, 768 (1962).

3. S. M. Sze and J. C. Irvin, "Resistivity, Mobility and Impurity Levels in GaAs, Ge and Si at 300 °K", Solid-State Electronics 11, 599 (1968).

4. G. Persky, "Thermionic Saturation of Diffusion Currents in Transistors", Solid-State Electronics 15, 1345 (1972).

5. S. M. Sze, "Physics of Semiconductor Devices", p. 94, Wiley (1969).

6. G. Siebert, "Increased Solar Cell Output by Improved Optical Matching", ESRO TN-90 (1969).

7. W. S. Johnson and J. F. Gibbons, "Projected Range Statistics in Semiconductors", Stanford Univ. Bookstore (1969).

8. Hunsperger, Wilson and Jamba, "Mg and Be Ion Implanted GaAs", J. Appl. Phys. 43, 1318 (1972).

9. C. J. Nuese and J. J. Gannon, "Electrolytic Removal of P-Type GaAs Substrates from Thin N-Type Semiconductor Layers", J. Electrochem. Soc. 117, 1094 (1970).

10. Wolfe, Stillman and Owens, "Residual Impurities in High-Purity Epitaxial GaAs", J. Electrochem. Soc. 117, 129 (1970).

11. J. Rachmann and R. Biermann, "Nachweis und Diffusion von Sauerstoff in GaAs", Solid State Comm. 7, 1771 (1969).

12. J. Vilms and J. P. Garrett, "Growth and Properties of LPE GaAs", Solid-State Electronics 15, 443 (1972).

13. J. M. Woodall and H. J. Hovel, "High-Efficiency Ga Al As - GaAs Solar Cells", Appl. Phys. Letters 21, 379 (1972).